Methylene- and ether-linked liquid crystal dimers II. Effects of mesogenic linking unit and terminal chain length

Peter A. Henderson[a]; John M. Seddon[b]; Corrie T. Imrie[a]

[a] Department of Chemistry, School of Engineering and Physical Sciences, University of Aberdeen, Meston Walk, AB24 3UE, UK [b] Department of Chemistry, Imperial College London, London SW7 2AZ, UK

PLEASE SCROLL DOWN FOR ARTICLE

Taylor & Francis
Taylor & Francis Group

Methylene- and ether-linked liquid crystal dimers II. Effects of mesogenic linking unit and terminal chain length

PETER A. HENDERSON†, JOHN M. SEDDON*‡ and CORRIE T. IMRIE*†

†Department of Chemistry, School of Engineering and Physical Sciences, University of Aberdeen, Meston Walk, Old Aberdeen, AB24 3UE, UK

‡Department of Chemistry, Imperial College London, Exhibition Road, London SW7 2AZ, UK

Four series of liquid crystal dimers have been prepared containing either ether-linked or methylene-linked spacers. Changing the spacer from being ether-linked, i.e. $O(CH_2)_nO$, to methylene-linked, i.e. $(CH_2)_{n+2}$, results in decreased nematic–isotropic transition temperatures, and this reduction is more pronounced for odd-membered spacers. By contrast, the entropy change associated with the nematic–isotropic transition is higher for an even-membered methylene-linked dimer than for the corresponding ether-linked material. This trend is reversed for odd members. These observations are completely in accord with the predictions of a theoretical model developed by Luckhurst and co-workers in which the only difference between the dimers is their shape. For the highly non-linear pentamethylene-linked dimers, only those with a short terminal chain exhibited fluid smectic behaviour, specifically, a monotropic alternating SmC structure which allowed for the efficient packing of the bent molecules. Once the terminal chain reached a value of $m=9$, a modulated ordered smectic phase was observed. For even-membered dimers, which exhibit only nematic phases upon melting for short terminal chain lengths, smectic phase behaviour was promoted with increasing terminal chain length, as is conventionally observed. Even-membered ether-linked dimers exhibited a SmC phase whereas even-membered methylene-linked dimers exhibited an ordered smectic G/J phase. Thus, it would appear that the differences in the transitional properties of ether- and methylene-linked dimers can be accounted for largely in terms of geometrical factors.

1. Introduction

Liquid crystal dimers consist of molecules containing two mesogenic units separated by a flexible spacer, most commonly an alkyl chain [1–3]. Dimers containing identical mesogenic units are referred to as symmetric dimers (see, for recent examples, [4, 5]) while non-symmetric dimers consist of two differing mesogenic groups (see, for recent examples, [6–10]). Although the most widely used spacer in dimers is an alkyl chain, other types of spacer including, for example, malonates [11], branched alkyl chains [12] and siloxanes [13, 14] have been utilized. The thermal behaviour of dimers containing alkyl spacers is quite different from that of conventional low molar mass mesogens; in particular, their transitional properties exhibit a pronounced alternation on varying the number and parity of methylene groups in the spacer [1–3]. Another structural

feature which has been varied in the dimeric architecture is the type of linking group between the spacer and mesogenic units including ethers [5], esters [15], thioesters [16] and thioethers [17].

The magnitudes of the odd–even effects seen for T_{NI} and $\Delta S_{NI}/R$ are also strongly dependent on the nature of the group linking the spacer to the mesogenic cores. Luckhurst and co-workers have suggested that the differences in the transitional behaviour of, for example, ether- and methylene-linked dimers arise from differences in molecular geometry and, specifically, from the bond angle between the *para* axis of the mesogen and the first bond in the spacer [18, 19]. For the methylene-linked dimers this bond angle is $113.5°$ while for ether-linked dimers it is $126.4°$. This difference makes the all-*trans* conformation of an ether-linked dimer more linear than that of the corresponding methylene-linked dimer. The greater shape anisotropy of the ether-linked dimers would be expected to give rise to higher nematic–isotropic transition temperatures. This view was supported by calculated T_{NI} values for the two series

*Corresponding author. Email: c.t.imrie@abdn.ac.uk; j.seddon@imperial.ac.uk

obtained using a molecular field theory [20] in which the only difference between the calculations for the two series was this bond angle [18]. The predictions of this theory were in good agreement with the experimental data, and furthermore it was shown that geometrical factors alone could also account for the differences in $\Delta S_{\mathrm{NI}}/R$ between ether- and methylene-linked dimers [19].

In a more transparent model developed by Luckhurst and co-workers, to understand how geometrical factors influence the transitional properties of dimers, the dimers can adopt just two conformations, one linear and one bent [21, 22]. This approach led to the intriguing prediction that systems containing high concentrations of bent conformers in the isotropic phase, i.e. dimers containing short odd-membered methylene-linked spacers, should exhibit a nematic–nematic transition [21, 22]. Indeed, the nematic–isotropic entropy exhibited by 1,5-bis(4-cyanobiphenyl-4′-yl)pentane is very small, suggesting that the transition is approaching second order in nature [23]. Theory suggests that following such a second order transition a biaxial nematic phase should be observed. Unfortunately, this possibility could not be investigated for this particular dimer because it exhibited a smectic phase, obscuring any possible nematic–nematic transition.

More recently, we described the properties of a range of odd- and even-membered methylene-linked dimers and compared these with the corresponding ether-linked dimers [24]. The transitional behaviour of the dimers did indeed agree with the theoretical predictions, although a biaxial nematic phase was not observed. However, an unusual alternating smectic C phase was observed, the driving force for which was suggested to be the highly non-linear molecular shape of the odd-membered methylene-linked dimers. In order to investigate the properties of these novel materials further we have synthesized and characterized two series of methylene-linked dimers, the α,w-bis(4-*n*-alkoxybenzylidineaniline-4′-yl)alkanes.
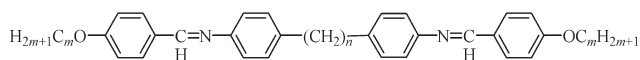
The acronym used to refer to these dimers is *m*O-*n*-O*m*, where *m* represents the number of carbon atoms in the terminal alkyloxy chain, and *n* the number of carbon atoms in the flexible spacer. For comparative purposes we also report the transitional behaviour of the corresponding ether-linked series, the α,ω-bis(4-*n*-alkoxybenzylidineaniline-4′-yloxy)alkanes:
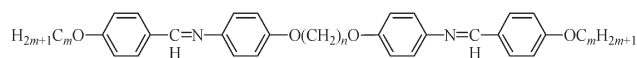
These are described using the acronym *m*O-O*n*O-O*m*. It should be noted that to make meaningful comparisons between these series we must compare dimers having the same number of atoms connecting the two mesogenic units, for example, 4O-5-O4 and 4O-O3O-O4. These particular series were chosen, in part, because the properties of the structurally similar α,ω-bis(4-*n*-alkylanilinebenzylidine-4′-yloxy)alkanes have been extensively investigated [25] and are referred to as the *m*.O*n*O.*m* series in which *m* denotes the length of the terminal alkyl chains, and *n* the length of the central flexible spacer.
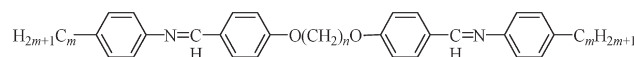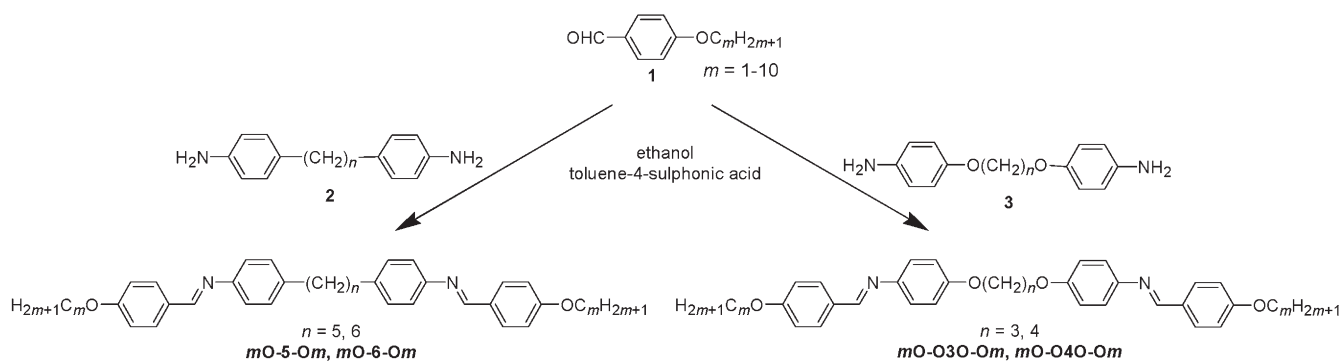

2. Experimental

2.1. *Synthesis*

The synthesis of each series of dimers is shown in scheme 1. The syntheses of the α,ω-bis(4-aminophenyl-4′-)alkanes and α-ω-bis(4-amoniphenyl-4′-oxy)alkanes have been described in detail elsewhere [24]. The first four members of the 4-*n*-alkoxybenzaldehyde series, **1**, were commercially available (Aldrich) and were redistilled immediately before use. The remaining members were prepared using the method described in detail in [26].

The syntheses of each dimer series were identical and a representative method is described for 1O-5-O1. Thus, 4-methoxybenzaldehye (1.3 mmol) was added to a stirred solution of 1,5-bis(4-aminophenyl-4′-)pentane (0.15 g, 0.60 mmol) containing a few crystals of toluene-4-sulphonic acid in hot ethanol. The reaction mixture was heated under reflux for 3 h. After cooling the resulting precipitate was filtered off, washed with cold ethanol, and recrystallized twice from ethanol. ^{1}H NMR (CHCl₃) δ (ppm): 8.4 (s, 2H, CH=N), 7.8 (d, 4H, Ar–H, *J*=8.25 Hz), 7.3–7.1 (m, 8H, Ar–H,), 7.0 (d, 4H, Ar–H, *J*=8.5 Hz), 3.9 (s, 6H, OC$\underline{H}_3$), 2.6 (t, 4H, ArC$\underline{H}_2$CH₃, *J*=7.5 Hz), 1.7 (qn, 4H, CH₂C$\underline{H}_2$CH₂C$\underline{H}_2$CH₂, *J*=7.5 Hz), 1.4 (m, 2H, CH₂CH₂C$\underline{H}_2$CH₂CH₂). IR *v* (cm^{-1}): 2912, 2849 (CH₂), 2849 (OCH₃), 3010, 1570 (conjugated C=N), 1606, 1510 (Ar–H), 821 (*p*-substituted aromatic).

All products were recrystallized twice from ethanol, except for the *m*O-O3O-O*m* series which were recrystallized twice from chloroform, and the *m*O-O4O-O*m* series which were recrystallized from mixtures of toluene and ethanol. Products were obtained in yields of 40–80%.

OHC⟶⟵OC$_m$H$_{2m+1}$
1   *m* = 1-10

H$_2$N⟶⟵(CH$_2$)$_n$⟶⟵NH$_2$
2

ethanol
toluene-4-sulphonic acid

H$_2$N⟶⟵O(CH$_2$)$_n$O⟶⟵NH$_2$
3

H$_{2m+1}$C$_m$O⟶⟵N=⟶⟵(CH$_2$)$_n$⟶⟵N=⟶⟵OC$_m$H$_{2m+1}$
n = 5, 6
*m*O-5-O*m*, *m*O-6-O*m*

H$_{2m+1}$C$_m$O⟶⟵N=⟶⟵O(CH$_2$)$_n$O⟶⟵N=⟶⟵OC$_m$H$_{2m+1}$
n = 3, 4
*m*O-O3O-O*m*, *m*O-O4O-O*m*

Scheme 1.   Synthesis of the dimer series.

2.2. Characterization

The proposed structures of the dimers were confirmed using a combination of ^{1}H NMR spectroscopy using a Bruker AC-F 250 MHz spectrometer, FTIR spectroscopy using an ATI Mattson Genesis Series FTIR spectrometer, and elemental analysis carried out by Butterworth Laboratories.

The thermal behaviour of the dimers was investigated by differential scanning calorimetry (DSC) using a Mettler Toledo DSC 820 differential scanning calorimeter equipped with a TS0801RO sample robot and calibrated using indium and zinc standards. The heating profile in all cases was heat, cool and reheat at $10°C \, min^{-1}$ with a 3 min isotherm between heating and cooling. All samples were heated from 0°C to 20–40°C above their clearing temperatures. Thermal data were normally extracted from the second heating trace. Phase characterization was performed using polarising optical microscopy using an Olympus BH2 polarising microscope equipped with a Linkam TMS 92 hot stage.

X-ray diffraction patterns were recorded using a Guinier camera fitted with a bent quartz monochromator (R. Huber, Germany) set to isolate Cu-K$_{\alpha 1}$ radiation ($\lambda = 1.5405$ Å) with non-aligned samples mounted in 2 mm thin-wall glass X-ray capillaries held in a thermostated sample holder. Some samples were measured using a home-built Guinier camera (courtesy of Dr V. Luzzati) and for these measurements the samples were mounted in metal cells with thin mica windows. The X-ray films were scanned using an Agfa Arcus II scanner at a resolution of 600 lines per inch, and processed using in-house developed Axcess X-ray analysis software (courtesy Mr A. Heron, Imperial College London). The spacings were calibrated using a silver behenate standard sample ($d = 58.3$ Å). The scattered intensities (arbitrary units), taken as the reciprocal optical transmission through the scanned X-ray film, were plotted against reciprocal spacing s (Å^{-1}) using Origin 7.0 (OriginLab Corporation). The

estimated accuracy of the X-ray layer spacing is ± 0.3 Å, and of the sample temperature is $\pm 1°C$.

3. Results and discussion

3.1. The *mO-O3O-Om* series

Table 1 lists the transition temperatures and associated entropy changes for the *m*O-O3O-O*m* series. In addition to the transitions listed in table 1 the homologues with *m*=5–10 also exhibited a weak endothermic crystal–crystal transition before melting. The methoxy, propoxy and butoxy members are monotropic nematogens while 2O-O3O-O2 shows an enantiotropic nematic phase. The nematic phase was assigned on the basis of the observation of characteristic schlieren textures containing both two- and four-point brush disclinations and which flashed when subjected to mechanical stress. The values of the entropy changes associated with the nematic–isotropic transitions for 1O-O3O-O1 and 2O-O3O-O2 are consistent with this assignment. The melting temperatures of 1O-O3O-O1 and 2O-O3O-O2 are in good agreement with published data, although the monotropic nematic phase was previously overlooked [27]. The dimers containing pentyloxy or longer terminal chains did not exhibit liquid crystal behaviour. A virtual N–I transition temperature of 119°C, i.e. approximately 30°C below the melting temperature, has been estimated for 6O-O3O-O6 by extrapolating the nematic-isotropic transition temperatures for mixtures of 6O-O3O-O6 and 2O-O3O-O2. 6O-O3O-O6 can only be supercooled, however, by approximately 20°C before crystallization.

The dependence of the transition temperatures on the number of carbon atoms, *m*, in the terminal alkyl chain for the *m*O-O3O-O*m* series is shown in figure 1. The melting point decreases as the length of the terminal chains is increased and appears initially to exhibit an odd–even effect. The nematic–isotropic transition temperatures exhibit an odd–even effect on increasing *m*,

Table 1. Transition temperatures and associated entropy changes for the *m*O-O3O-O*m* series. Monotropic transition temperatures are given in ( ). [ ] Refers to a virtual transition temperature obtained by extrapolation of the T_{NI} curve for mixtures of 6O-O3O-O6 and 2O-O3O-O2.

m	T_{CrI}, T_{CrN}/ °C	T_{NI}/ °C	$\Delta S_{CrI}/R$, $\Delta S_{CrN}/R$	$\Delta S_{NI}/R$
1	188	(175)	17.7	0.28
2	177[a]	186	16.1[a]	0.39
3	181	(157)	19.0	—
4	174	(160)	19.3	—
5	168	—	19.6	—
6	163	[119]	20.0	—
7	160	—	20.9	—
8	158	—	21.4	—
9	155	—	22.1	—
10	153	—	22.4	—

[a]Crystal–nematic transition.

which is typical behaviour for liquid crystal dimers [25]. It is clear that T_{NI} decreases more rapidly than the melting point with increasing *m*, and hence no liquid crystalline behaviour is observed for the higher homologues.

The value of the melting entropy ($\Delta S/R$) tends to increase on ascending the series, suggesting that for the higher members there is a greater conformational contribution to the entropy change arising from the melting of the longer terminal chains. This accounts also for the decrease in the melting point on ascending the series. The value for the ethoxy derivative does not fit this general trend as this exhibits a Cr–N rather than a Cr–I transition.

As we noted earlier, a structurally similar series of dimers to the *m*O-O3O-O*m* series, the α,ω-bis(4-alkylanilinebenzylidene-4′oxy)alkanes (*m*.O*n*O.*m*) have been extensively investigated [25]. These differ from the *m*O-O3O-O*m* series in that the direction of the Schiff's base linkage is reversed and the terminal alkyl chains are linked directly to the mesogenic units. For conventional low molar mass mesogens the reversal of the Schiff's base link in the mesogenic core has little effect upon transitional behaviour and there is no apparent reason why this should not also be the case for dimers. Thus, differences in transition temperatures between these two series may be attributed largely to the effects of the ether link in the terminal chain.

Members of the *m*.O3O.*m* series exhibit lower transition temperatures than the corresponding *m*O-O3O-O*m* homologue and display a greater variety of liquid crystal phases. The first four members of the *m*.O3O.*m* series (*m*=1–4) are monotropic nematogens. The remaining compounds exhibit a SmA phase which changes from being monotropic to enantiotropic in nature at *m*=6. Compounds 9.O3O.9 and 10.O3O.10 also exhibit a SmC phase, with the latter also showing a monotropic SmF phase. The observation of these phases may be attributed, at least in part, to the lower melting temperatures of the *m*.O3O.*m* compounds, which do not obscure the observation of liquid crystalline behaviour as is presumably the case for the *m*O-O3O-O*m* series. In addition, it should be noted that members of the *m*.O3O.*m* series can be supercooled to a greater extent than those of the *m*O-O3O-O*m* series. These observations suggest that for the *m*O-O3O-O*m*
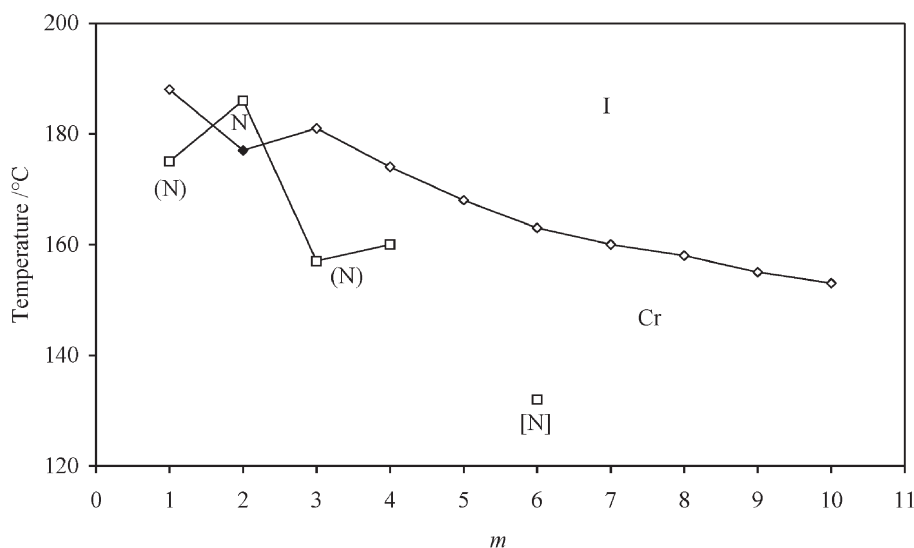

Figure 1. Dependence of transition temperature on the increasing number of carbon atoms, *m*, in the terminal alkoxy chains for the *m*O-O3O-O*m* series. (◇) Cr–I, (◆) Cr–N, (□) N–I. Monotropic phases are denoted by ( ) and a virtual transition temperature by [ ].

Table 2. Transition temperatures and associated entropy changes for the *m*O-5-O*m* series. Monotropic transition temperatures are given in ( ) and were obtained using microscopy. X refers to a modulated ordered smectic phase related to the G/J phase (see text).

m	T_{Cr}/ °C	T_{SmN}/ °C	T_{NI}, T_{XI}/ °C	ΔS_{Cr}/ R	ΔS_{XI}/ R
1	123	(83)	(86)	11.0	—
2	130	(106)	(107)	10.8	—
3	117	—	—	10.8	—
4	120	—	(113)	10.8	—
5	116	—	—	6.1	—
6	121	—	—	7.9	—
7	120	—	—	8.2	—
8	121	—	—	8.3	—
9	97	—	118[a]	13.6	9.1
10	97	—	118[a]	12.0	9.9

[a]Smectic X–isotropic transition.

series, the ether links between the terminal chains and mesogenic groups increase the shape anisotropy of the dimer, thus enhancing both molecular associations and the packing of the molecules, resulting in higher melting temperatures and a reduced tendency to supercool without crystallizing.

3.2. *The m*O-5-O*m series*

Table 2 lists the transition temperatures and associated entropy changes for the *m*O-5-O*m* series. All members of the series also exhibit one or two weak endothermic crystal–crystal transitions prior to melting.

Compounds 1O-5-O1 and 2O-5-O2 exhibit monotropic nematic and smectic phases [24]. An earlier report describing 1O-5-O1 appears to have overlooked the monotropic liquid crystalline behaviour [28]. The smectic phase exhibited by 1O-5-O1 and 2O-5-O2 was assigned as an alternating smectic C phase, although its

monotropic nature precluded detailed study by XRD [24]. 4O-5-O4 is also a monotropic nematogen although the nematic phase can only be supercooled by a few degrees before crystallization.

The propyloxy and pentyloxy to octyloxy members melt directly into the isotropic phase. By comparison, the DSC traces of 9O-5-O9 and 10O-5-O10 reveal two strong endothermic transitions on heating: the first at 97°C to a mesophase, followed by a transition to the isotropic phase at 118°C. The initial crystal phase of 9O-5-O9 has a measured layer spacing of 45.9 Å (diffraction orders 1, 2 and 6 observed), which is slightly less than the estimated molecular length of 48.5 Å, implying a tilt angle of 19°. On heating above 97°C, the layer spacing drops abruptly to 41.3 Å, and the wide angle pattern now consists of a small number of sharp lines in the region of 4.2–4.8 Å, consistent with a tilted ordered smectic phase. The layer spacing implies a tilt angle of *c.* 31°. It is noteworthy that an additional sharp low angle line at a spacing of 23.2 Å (very close to the second order peak of the lower temperature crystal phase) is present across the whole range of the ordered smectic phase, suggesting that it has a modulated structure, rather than a simple layer stacking (see later). The optical texture exhibits broken and chunky focal-conic fans with distinct grain boundaries, see figure 2 (*a*). The phase is viscous but can be sheared to give a schlieren texture. The phase is assigned as a modulated ordered smectic phase, related to the G/J phases.

The G/J phases can be described as 3D ordered versions of the tilted hexatic phases smectic F/I. For the G and F phases, the molecular tilt lies towards the face of the local hexagonal net (halfway between nearest neighbours), whereas for the J and I phases, the tilt lies towards the hexagon apex (nearest neighbour direction). The coupling between the layers for the ordered
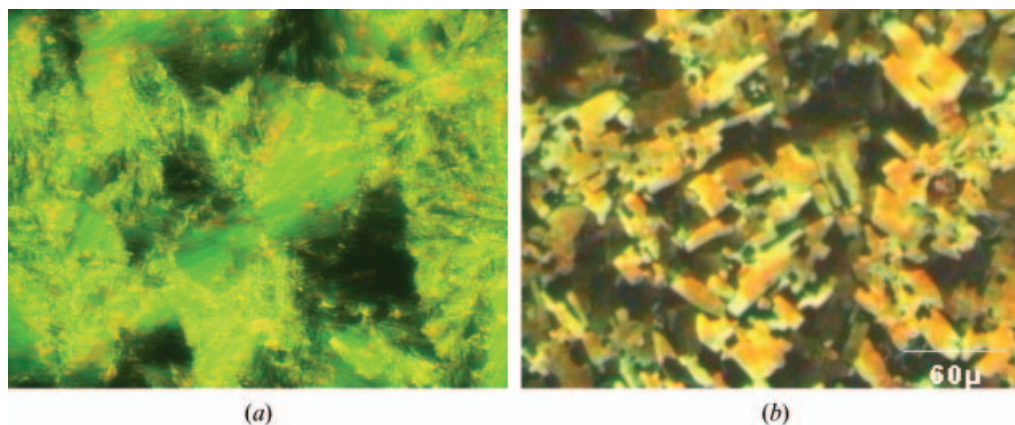

Figure 2. Optical textures of (*a*) 9O-5-O9 at 112°C and (*b*) 10O-5-O10 at 114°C.

G/J phases means that the six-fold rods of diffuse wide angle scattering observed in the hexatic F/I phases, centred at the $2\,0\,0$ and $1\,1\,0$ positions (indexing the phases as *C*-face-centred monoclinic), condense into rows of sharp $h\,k\,l$ Bragg peaks, the molecular form factor usually causing the $h\,k\,0$ peaks to be the most intense, surrounded by weaker satellite $h\,k\,l$ peaks. When molecular tilt is present, these satellite reflections are distributed on either side of the position of the main peak from the hexagonal (or close to hexagonal) packing of the molecules, which occurs at a spacing of approximately $4.5\,\text{Å}$ (in the absence of tilting, the $h\,k\,l$ satellite peaks would all appear at slightly larger diffraction angles—lower spacings—than the $2\,0\,0/1\,1\,0$ peak at a spacing of $4.5\,\text{Å}$).

The crystal phase exhibited by 10O-5-O10 has a lamellar structure (diffraction orders 1, 2, 3, 4 and 6 observed) with a layer spacing of $48.8\,\text{Å}$. When compared with the calculated molecular length of $50.9\,\text{Å}$, this implies a tilt angle within the crystalline layers of $16.5°$. The mesophase adopted by 10O-5-O10 above $97°$C has a very similar X-ray pattern to that seen for the ordered smectic phase of 9O-5-O9, but with a layer spacing of $45.3\,\text{Å}$, or $4\,\text{Å}$ larger. Again, an additional sharp low angle line, at a spacing of $23.2\,\text{Å}$, very close to the second order peak of the crystal phase, is present across the whole range of the ordered smectic phase. In addition a very weak, slightly diffuse line is seen at a spacing of $34.8\,\text{Å}$. This confirms that the ordered smectic phase of both pentamethylene-linked dimers must have a modulated structure. A lengthy exposure of the phase at $108°$C using the 'Luzzati' camera showed a layer spacing of $46.7\,\text{Å}$, along with the 2nd, 3rd, 4th and 6th order reflections of a $48.6\,\text{Å}$ repeat spacing, as well as weak, slightly diffuse lines at 35.3 and $19.8\,\text{Å}$ (see figure 3). A number of lines were observed in the wide angle region, within the spacings range of $4.0–4.9\,\text{Å}$, the strongest being at 4.46 and $4.55\,\text{Å}$, with three weak lines observed at slightly lower angles and four at slightly higher angles. The observation of two strong wide angle lines close to a spacing of $4.5\,\text{Å}$ implies a slight deviation of the molecular cross-sectional packing away from 2D hexagonal. The optical texture of this phase consists of elongated platelets with distinct boundaries, see figure 2(*b*). This phase is assigned as an ordered smectic phase having a modulated layer structure, related to the more usual G/J phases.

The dependence of the transition temperatures on the length of the terminal alkyl chains for the *m*O-5-O*m* series is shown in figure 4. The melting points exhibit a weak odd–even effect which attenuates slightly with increasing *m*. There is only a small decrease in the
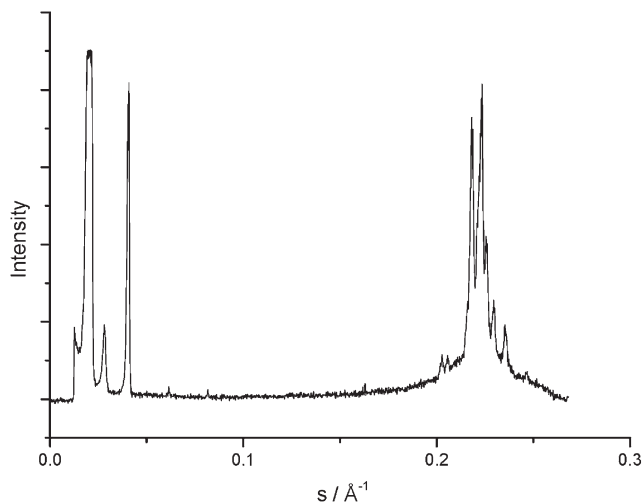

Figure 3. X-ray powder pattern of the modulated ordered smectic phase of 10O-5-O10 at 108°C . The lowest angle peak is broadened because it is over-exposed.

melting temperature on ascending the series, but these temperatures are all considerably lower than those of the corresponding members of the *m*O-O3O-O*m* series. The only members of the *m*O-5-O*m* series to exhibit smectic behaviour are 1O-5-O1 and 2O-5-O2. For the *m*.O*n*O.*m* family of compounds smectic behaviour is only observed if the length of the terminal chains is greater than half the length of the spacer [25] and a similar relationship has been observed for other symmetric dimers [29]. As we will see, the behaviour of the *m*O-O*n*O-O*m* series is also in accord with these observations. Thus, the observation of smectic behaviour for 1O-5-O1 and 2O-5-O2 is most surprising and we will return to this later.

3.3. *The* m*O-O4O-O*m *series*

The transition temperatures and associated entropy changes for the *m*O-O4O-O*m* series are listed in table 3. All the members of the series exhibit one or two weak endothermic crystal–crystal transitions before melting and each exhibits enantiotropic liquid crystalline behaviour.

The first seven homologues are exclusively nematogenic while the decyl, undecyl and dodecyl members show only a smectic C phase. The SmC phase is assigned on the basis of the observation of an optical texture containing focal conic fans which shear to give a schlieren texture, see figure 5. Microscope studies on freestanding films reveal a schlieren texture also indicating that the phase is tilted.

Figure 6 shows the dependence of the transition temperatures on terminal chain length for the *m*O-O4O-O*m* series. The nematic–isotropic transition
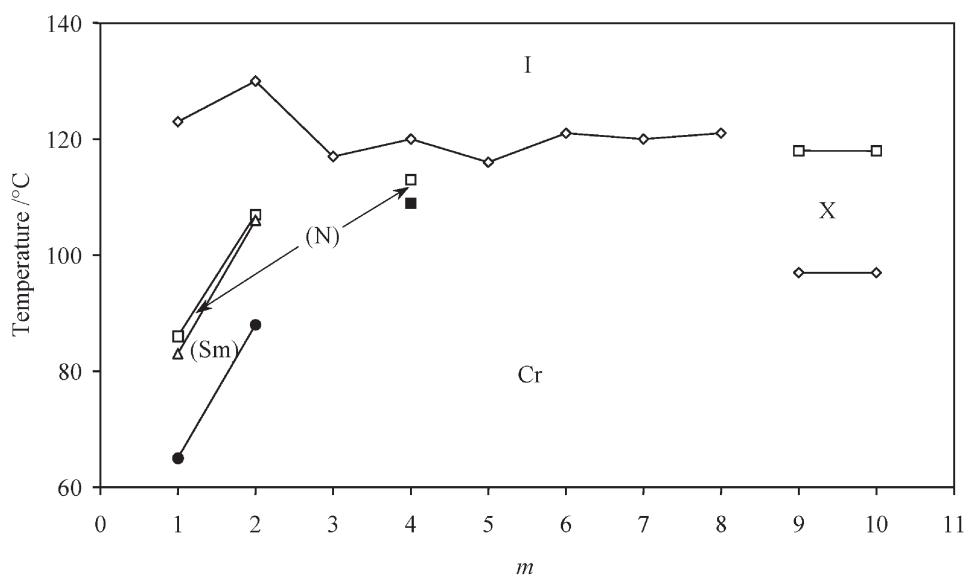
Figure 4. Dependence of transition temperature on the number of carbon atoms, *m*, in the terminal alkoxy chains for the *m*O-5-O*m* series. (◇) Cr–I, Cr–X, (□) N–I, (■) N–Cr, (△) Sm–N, (●) Sm–Cr. X refers to an ordered smectic phase having a modulated layer structure, related to the G/J phases.

temperatures initially show a small odd–even effect which rapidly attenuates. The melting temperatures of the first two members are similar; the melting temperature then increases, before falling on further increase of the chain length.

$\Delta S_{NI}/R$ values for the first four members of the series are large but typical for even-membered liquid crystal dimers. The decrease in $\Delta S_{NI}/R$ on passing from 4O-O4O-O4 to 5O-O4O-O5, and the subsequent decrease seen for the hexyl and heptyl members, are due to an overlap of the melting and clearing peaks in the DSC traces leading to an underestimation of the clearing entropy value. The larger clearing entropies for the final three compounds reflect the switch from a nematic–isotropic to a smectic C–isotropic clearing transition

and the resolution of the melting and clearing peaks in the DSC trace, although $\Delta S_{SmCI}/R$ for 8O-O4O-O8 is surprisingly low.

XRD data for 9O-O4O-O9 and 10O-O4O-O10 show layer spacings in the crystal phase of 45.3 and 49.7 Å, respectively, which from the estimated molecular lengths of 47.7 and 50.5 Å, implies tilt angles of 18° and 10°. The smectic phase of 10O-O4O-O10, adopted above 184°C, gives only diffuse wide angle scattering, indicative of a fluid phase, and has a layer spacing of 42.5 Å implying a tilted phase with a tilt angle of

Table 3. Transition temperatures and associated entropy changes for the *m*O-O4O-O*m* series.

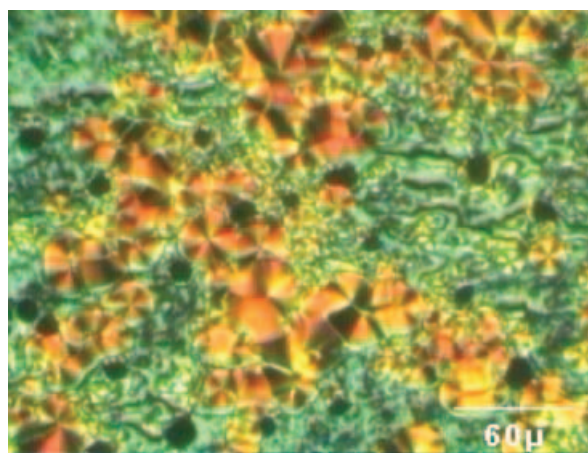| *m*	$T_{Cr}/$ °C	$T_{NI}, T_{SmCI}{}^{a}/$ °C	$\Delta S_{Cr}/R$	$\Delta S_{NI}/R, \Delta S_{SmCI}/R^{a}$
1	212	239	8.29	0.97
2	210	240	10.3	1.15
3	221	234	8.80	1.69
4	215	233	10.1	1.88
5	206	214	11.9	0.75
6	198	204	10.7	0.35
7	194	203	12.9	0.35
8	190	202[a]	10.4	0.90[a]
9	188	203[a]	12.6	2.19[a]
10	184	204[a]	13.2	5.35[a]

[a]Smectic C–isotropic transition.

Figure 5. Smectic C phase of 10O-O4O-O10 at 204°C showing focal conic fans in coexistence with regions of schlieren texture.
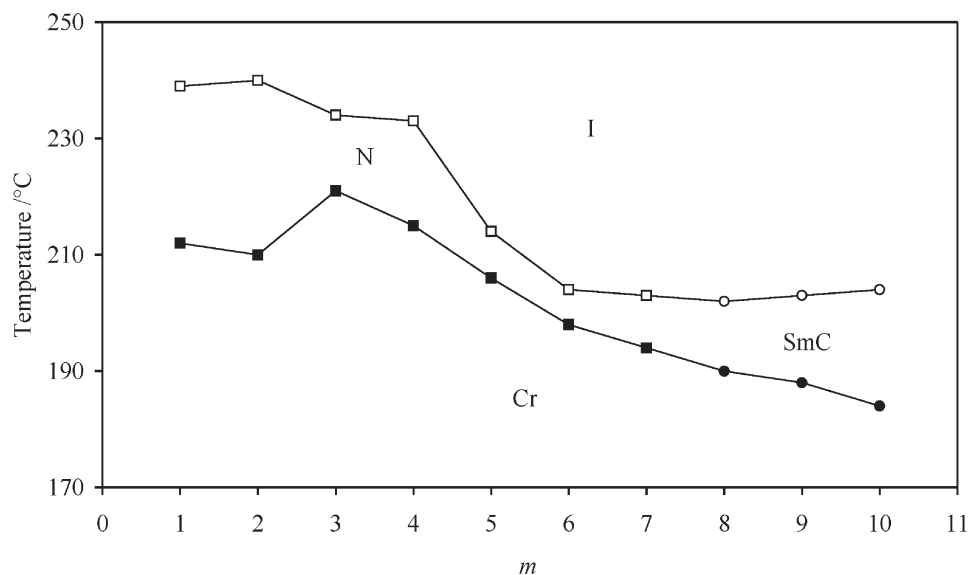
Figure 6. Dependence of transition temperature on the number of carbon atoms, *m*, in the terminal chain for the *m*O-O4O-O*m* series. (■) Cr–N, (□) N–I, (●) Cr–SmC, (○) SmC–I.

approximately 33°. Thus the X-ray data are consistent with the assignment of a smectic C phase.

3.4. *The* m*O-6-O*m *series*

The transition temperatures and associated entropy changes for the *m*O-6-O*m* series are listed in table 4. All the compounds in this series are enantiotropic nematogens, and in addition, smectic behaviour emerges at 5O-6-O5. The DSC reheat traces are collected in figure 7. The DSC traces and POM studies reveal the existence of either one or two additional phases as well as the nematic phase for compounds having pentyl or longer terminal chains. Each of these will be discussed in detail later.

Figure 8 shows the dependence of the transition temperature on the length of the terminal alkyl chains for the *m*O-6-O*m* series. The melting point is similar for the first four members and then decreases before levelling out again after *m*=7. The nematic–isotropic transition temperature increases on passing from 1O-6-O1 to 2O-6-O2 and then decreases gradually on increasing the chain length. As *m* is increased the temperature range of the nematic phase is reduced while that of the smectic or disordered crystal phase increases. The G/J–N and N–I transitions could not be resolved for *m*=9, as shown in table 4. We will compare the properties of the *m*O-O4O-O*m* and *m*O-6-O*m* series later.

Materials with *m* greater than 5 show several large endothermic peaks in their reheating and cooling DSC traces before the transition into the nematic phase. As can be seen in figure 7 the two lower temperature transitions merge as *m* is increased. The nematic phase region also becomes narrower as *m* is increased, resulting in an enlargement of the temperature range

Table 4. Transition temperatures and associated entropy changes for the *m*O-6-O*m* series.

m	T_{Cr}/°C	$T_{CrG/J}$/°C	$T_{G/JN}$/°C	T_{NI}/°C	$\Delta S_{Cr}/R$	$\Delta S_{CrG/J}/R$	$\Delta S_{G/JN}/R$	$\Delta S_{NI}/R$
1	140	—	—	214	9.9	—	—	2.21
2	134	—	—	223	9.0	—	—	2.71
3	131	—	—	206	7.6	—	—	2.40
4	135	—	—	196	6.4	—	—	2.43
5	70	117	153	192	4.5	3.03	3.66	2.61
6	78	102	154	186	8.7	3.87	2.58	2.68
7	86	—	169	183	(14.9)	—	3.75	2.72
8	85	—	174	181	9.8	—	3.37	2.89
9	91	—	173	177	(18.6)	—	7.80[a]	
10	90	—	171	176	(17.7)	—	2.05	5.29

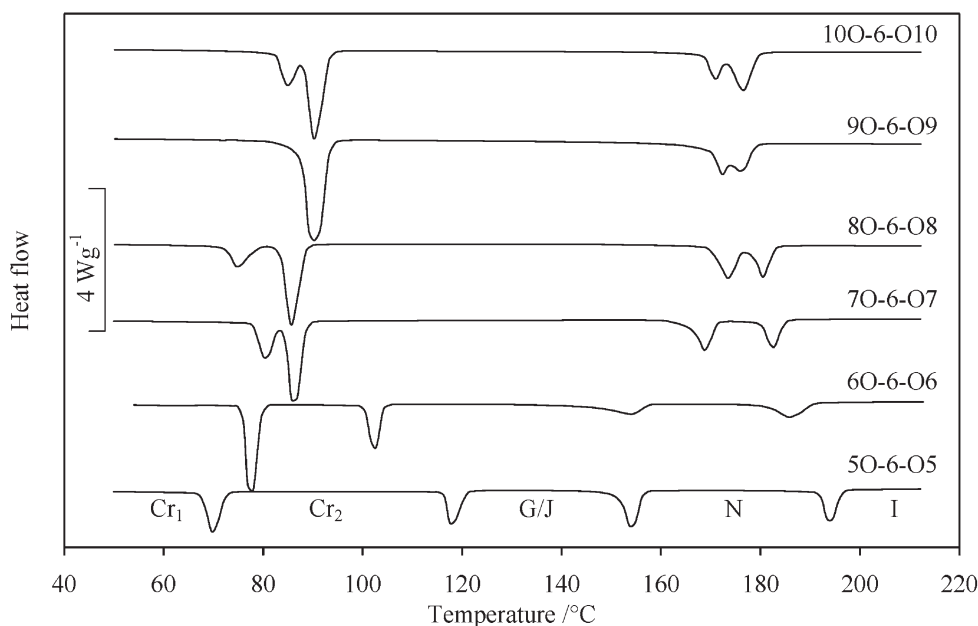[a]Combined G/J-N and N-I entropy values.

Figure 7. Normalized DSC traces for the members of the *m*O-6-O*m* series exhibiting polymorphism.

of the intermediate phase. The phase structures of several of these materials were studied further by XRD.

3.4.1. 5O-6-O5. XRD studies using both the Huber variable temperature and Luzzati fixed temperature instruments were performed on 5O-6-O5. The Huber scan of the crystal phase shows a layered structure with 1st and 2nd order reflections corresponding to a *d*-spacing of 28.1 Å, much less than the estimated

molecular length of 38.6 Å. An exposure taken with the Luzzati camera at 60°C showed a mixture of the 28.1 Å crystal phase, with another crystal phase of spacing 20.1 Å, indicative of low temperature crystalline polymorphism. The diffraction pattern from the phase formed above 70°C revealed a layered structure, with a *d*-spacing of 28.7 Å as measured by the Huber camera. A longer exposure with the Luzzati camera at 100°C gave a layer spacing of 29.6 Å, and numerous lines in
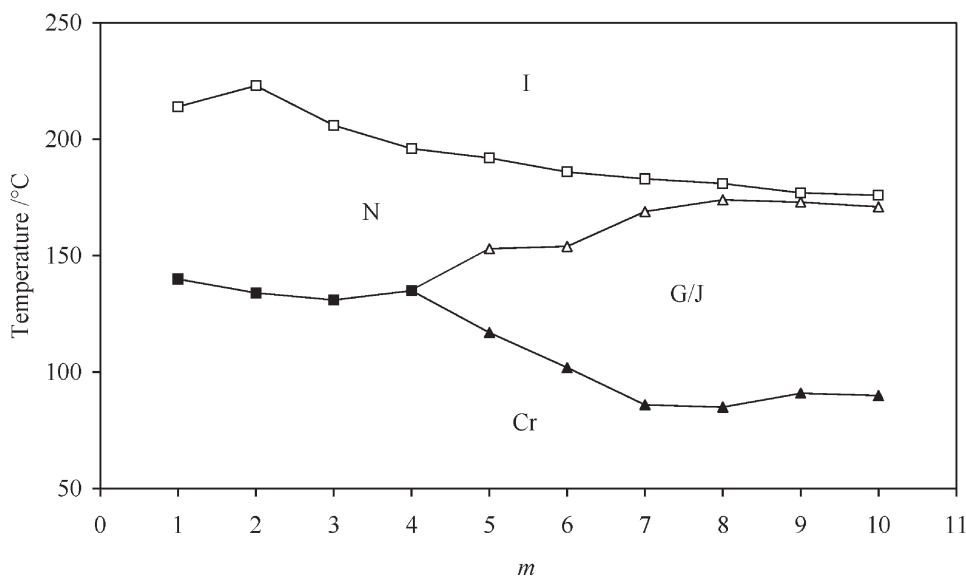

Figure 8. Dependence of transition temperature on the number of methylene units, *m*, in the terminal alkyl chain for the *m*O-6-O*m* series. (■) Cr–N, (▲) Cr–G/J, (△) G/J–N and (□) N–I.
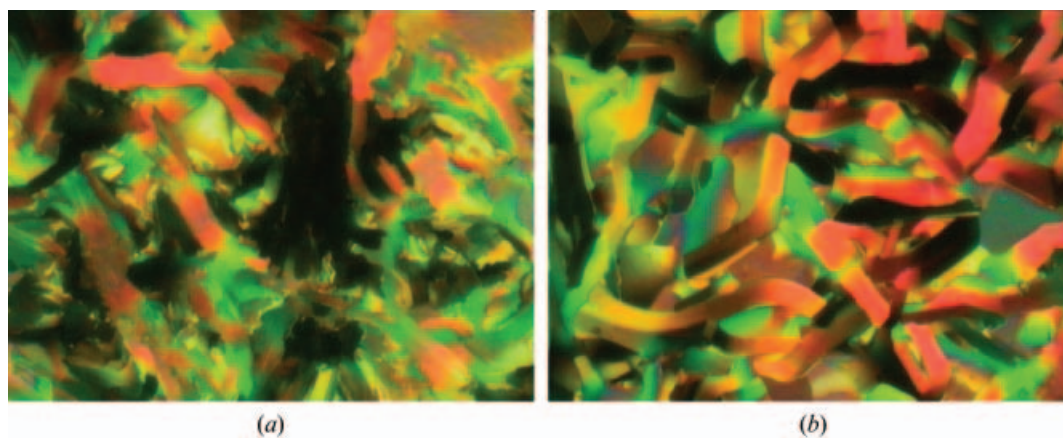
Figure 9.   Optical textures of 5O-6-O5. (*a*) Second crystal phase at 100°C and (*b*) crystal G/J phase at 145°C.

the wide angle region, proving that this is a second crystal phase. The phase exhibits a mosaic texture and is extremely viscous, see figure 9 (*a*).

The higher temperature phase formed above 117°C also shows a layered structure, with a *d*-spacing of 33.2 Å from the Luzzati camera at 140°C, see figure 10. This value suggests a tilted phase with a tilt angle of *c.* 33.5°. The wide angle region shows a strong peak at 4.5 Å plus seven weak reflections on either side of it with spacings in the range 4–5 Å, indicating that this is a tilted ordered smectic phase. Under the microscope on transition to this phase the platelets appear more rounded and blemishes on the platelets disappear, see figure 9 (*b*). This phase is tentatively assigned as a G/J phase.

3.4.2.   6O-6-O6. The crystal phase of 6O-6-O6 shows a lamellar structure with a relatively short periodicity of
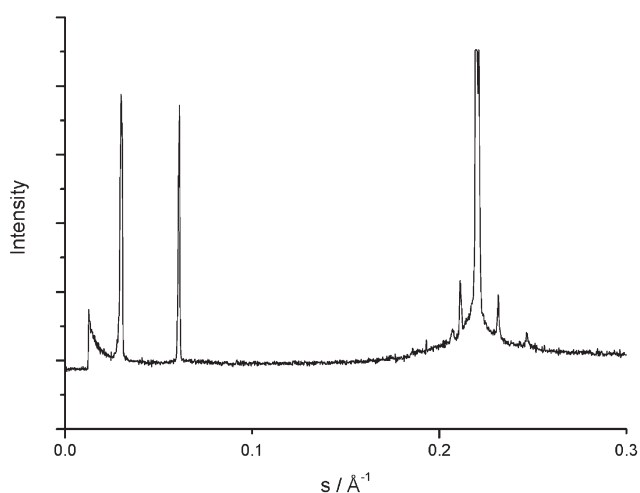

Figure 10.   X-ray powder pattern of the ordered smectic phase of 5O-6-O5 at 140°C.

~20 Å which is approximately half the calculated molecular length of 41.5 Å. The phase obtained after the first melting transition shows a mosaic texture, with elongated lined platelets, see figure 11 (*a*), and has a *d*-spacing of 28.6 Å. The numerous reflections in the wide angle region show this to be a second crystal phase. The higher temperature mesophase also has a layered structure with a further increase of the *d*-spacing to 34.3 Å. Two strong lines are seen in the wide angle region at 4.44 and 4.48 Å, with weaker satellite reflections on either side, again similar to the pattern for 5O-6-O5. The elongated platelets seen in the optical texture of this phase become smoother with more rounded ends at the transition from the crystal phase that precedes it, see figure 11 (*b*), and can be sheared to form a schlieren texture. This phase is assigned as a crystal G/J phase.

3.4.3.   7O-6-O7. The crystal phase of 7O-6-O7 shows a lamellar structure with a *d*-spacing of 42.8 Å, which is slightly less than the molecular length of 43.2 Å, see figure 12. On heating, the resulting phase also has a lamellar structure with a slight decrease in the *d*-spacing to 39.2 Å, suggesting a tilted phase. The number of reflections in the wide angle region indicates a crystal phase. POM reveals a mosaic texture with fairly rounded, lined platelets, see figure 13 (*a*).

The next, higher temperature mesophase also shows a lamellar structure, again with a decrease of the *d*-spacing to 35.4 Å. There is a strong wide angle reflection at 4.43 Å with weak sharp lines either side at 4.70 and 4.11 Å, suggesting a tilted ordered smectic phase. The optical texture exhibits rounded platelets, figure 13 (*b*). This phase is also assigned as a crystal G/J phase. The optical textures of the higher temperature phase immediately preceding the nematic phase of 8O-6-O6 and 9O-6-O9 are shown in figures 13 (*c*) and 13 (*d*),
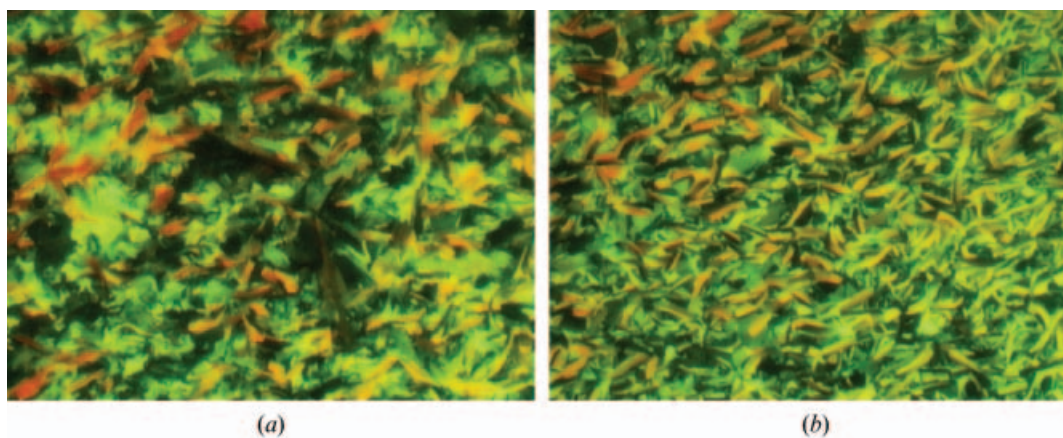
Figure 11. Optical textures of 6O-6-O6. (*a*) High temperature crystal phase at 89°C and (*b*) G/J phase at 135°C.

respectively. These are similar to that of 7O-6-O7, and hence are also assigned as G/J phases.

3.4.4. 10O-6-O10.

The X-ray diffraction patterns of 10O-6-O10 are similar to those of 7O-6-O7. Thus, the crystal phase shows a lamellar structure and reflections of order 1, 2, 3, 4 and 6 are seen giving a *d*-spacing of 50.1 Å, which is comparable to the calculated molecular length of 50.7 Å. On melting, the resulting phase contains 1st and 2nd order reflections in the small angle region giving a *d*-spacing of 45.3 Å. The wide angle region contains several reflections indicating a crystalline phase. The higher temperature phase also shows a layered structure but with a further reduction in the *d*-spacing to 43.1 Å, implying a tilt angle within the phase of 31.9°. The strong wide angle peak at 4.44 Å, with weak sharp satellite lines at 4.18 and 4.57 Å, suggests a tilted ordered smectic phase. The optical textures obtained for this phase are shown in figure 14. The texture consists of regions of curved, lined fans, (*a*), as well as a mosaic texture, (*b*). Thus, this phase is also assigned as a crystal G/J phase.

3.5. Comparison of the four series

The melting temperatures of the *m*O-O*n*O-O*m* and *m*O-*n*-O*m* series are compared in figure 15. The *m*O-O4O-O*m* series has the highest melting temperatures, as may be expected, as these are the most linear of the dimers studied and this enhanced linearity presumably allows efficient packing in the crystal phase. The melting temperatures for the *m*O-O3O-O*m* series are lower than those of the corresponding even membered dimers, and this difference in temperature is almost constant across the series. This reduction in melting point is expected, as the odd-membered dimers have a reduced shape anisotropy. The melting points of the *m*O-O3O-O*m* series are higher than those of the corresponding *m*O-6-O*m* dimers, indicating that shape alone cannot account for the melting temperature. Presumably the enhanced molecular interactions arising from having the ether-linked spacer increases the melting points in the *m*O-O*n*O-O*m* series. The *m*O-5-O*m* series exhibits the lowest melting temperatures for low values of *m*, but for values of *m* above 5 the *m*O-6-O*m* dimers show the lowest melting points. This crossover in the melting
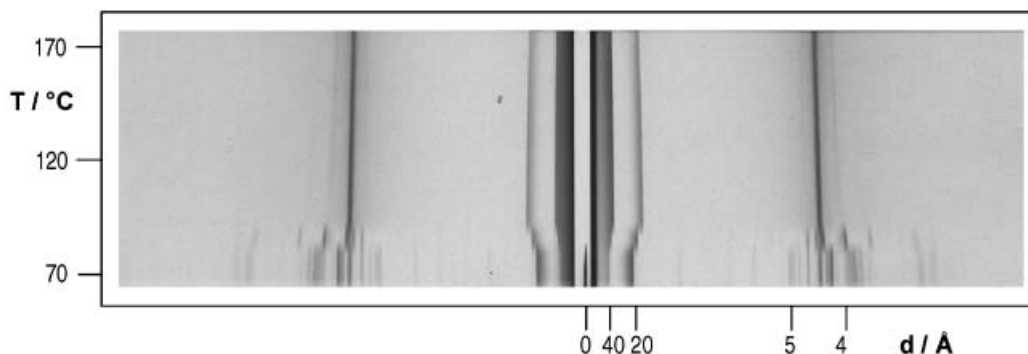

Figure 12. An X-ray temperature scan of 7O-6-O7 showing two crystal phases followed by an ordered smectic phase upon heating. The heating rate was $10°C\,h^{-1}$.
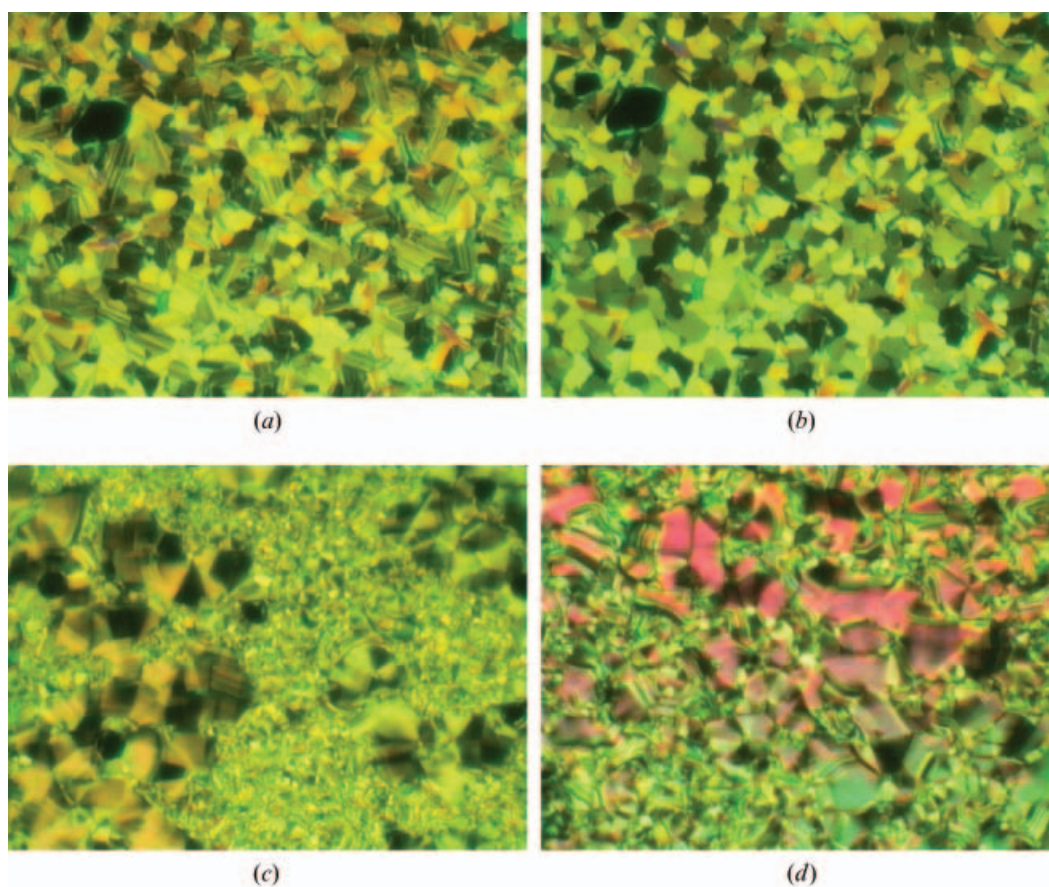
Figure 13.   Optical textures of 7O-6-O7: (*a*) High temperature crystal phase at 85°C and (*b*) G/J phase at 150°C. The disordered crystal phase of (*c*) 8O-6-O8 at 153°C and (*d*) 9O-6-O9 at 130°C.

temperatures arises from the classification of the ordered smectic mesophase for the *m*O-6-O*m* series, and thus we are no longer comparing like transitions. The melting temperatures of both ether-linked series are higher than those for the methylene-linked dimers, and the reduction in melting temperature is greatest for the even-membered dimers. This presumably arises from a subtle interplay of the effects of changing the molecular shape and the molecular interactions on switching from ether to methylene links.

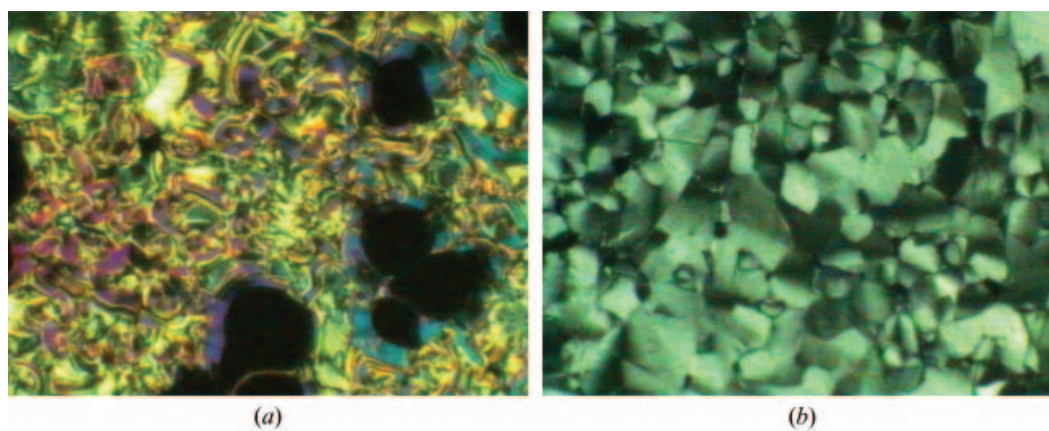The clearing temperatures of the four dimer series are shown in figure 16. The even-membered ether-linked

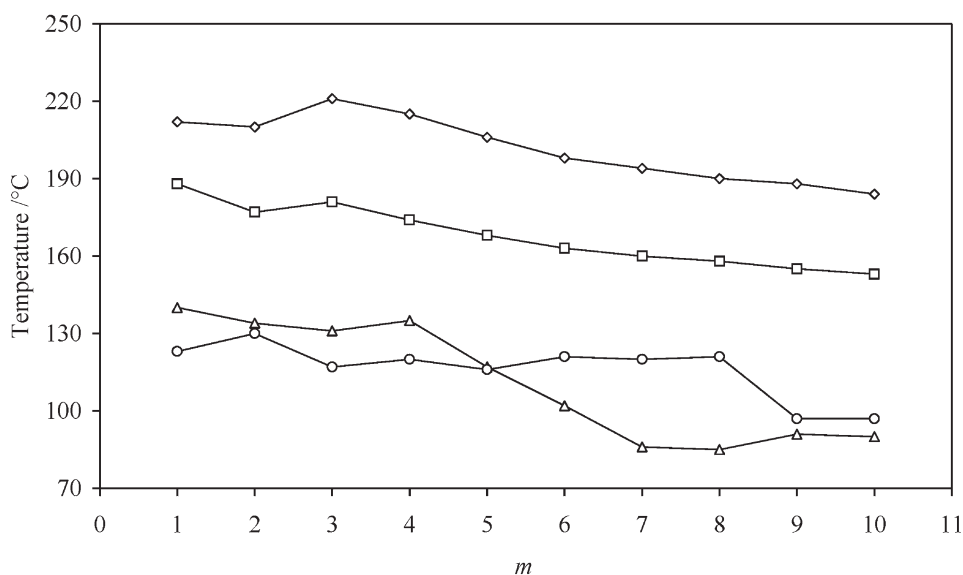Figure 14.   Optical textures of 10O-6-O10 at 140°C.

Figure 15. Dependence of melting temperature on the terminal chain length for the (◇) mO-O4O-Om, (□) mO-O3O-Om, (△) mO-6-Om and (○) mO-5-Om series.

mO-O4O-Om series has the highest clearing temperatures, and the lowest are exhibited by the mO-5-Om series. The even-membered dimers all have higher clearing temperatures than those of the corresponding odd-membered dimers and the ether-linked dimers have higher clearing temperatures than those of the corresponding methylene-linked dimers. Changing from an even-membered to an odd-membered spacer leads to a greater reduction in the clearing temperature than does replacing an ether link with a methylene link. This may suggest that molecular shape plays a more important role in determining T_{NI} than it does in determining the melting temperature.

It is difficult to compare the transition entropies between the series because of the different transitional behaviour. Where comparisons are possible, however, the observed behaviour is in agreement with the predictions made by Luckhurst and co-workers [18, 19, 22], i.e. changing the spacer from being ether-linked to methylene-linked results in decreased
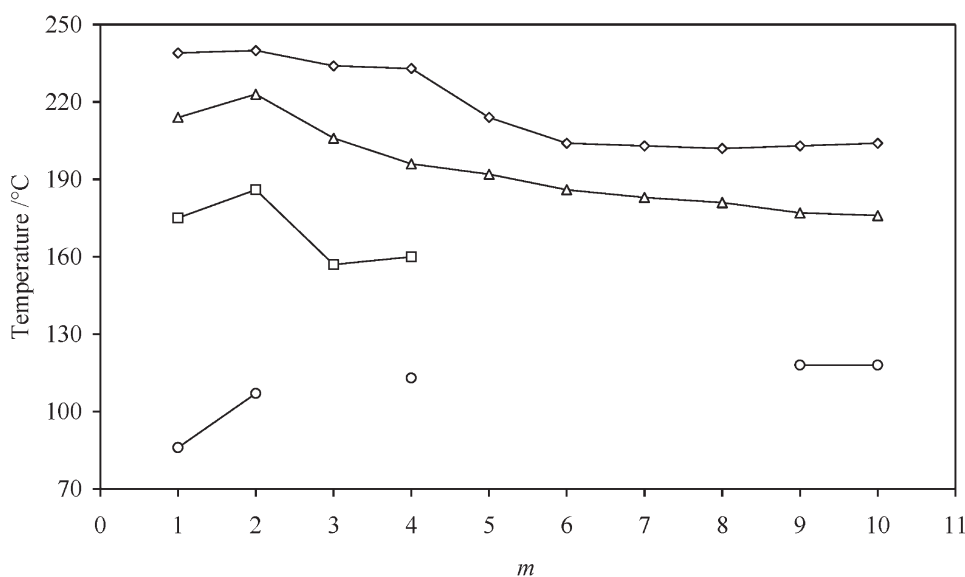

Figure 16. Dependence of clearing temperature on the terminal chain length for the (◇) mO-O4O-Om, (△) mO-6-Om, (□) mO-O3O-Om, and (○) mO-5-Om series.

nematic–isotropic transition temperatures and this reduction is more pronounced for odd-membered spacers. By contrast, the entropy change $\Delta S_{NI}/R$ is higher for an even-membered methylene-linked dimer than for the corresponding ether-linked material, with this trend being reversed for odd members.

4. Conclusions

Four series of liquid crystal dimers have been prepared containing either ether-linked or methylene-linked spacers. Changing the spacer from being ether-linked, i.e. $O(CH_2)_nO$, to methylene-linked, i.e. $(CH_2)_{n+2}$, results in decreased nematic–isotropic transition temperatures and this reduction is more pronounced for odd-membered spacers. By contrast, the entropy change associated with the nematic–isotropic transition is higher for an even-membered methylene-linked dimer than for the corresponding ether-linked material. This trend is reversed for odd members. These observations are completely in accord with the predictions of a theoretical model developed by Luckhurst and co-workers [18, 19, 22] in which the only difference between the dimers is their shape. In addition, only highly non-linear pentamethylene-linked dimers exhibited smectic C behaviour and, specifically, an alternating structure which allowed for the efficient packing of the bent molecules. Thus, it would appear that the differences in the transitional properties of ether- and methylene-linked dimers can be accounted for largely in terms of geometrical factors.

The ether-linked dimers studied here exhibit only nematic phases (usually monotropic) for an odd parity spacer ($n=3$), but for an even parity spacer ($n=4$), the nematic phase changes to a smectic C phase when the terminal chain $m>7$.

For the methylene-linked dimers, those with an odd parity spacer ($n=5$) exhibit monotropic nematic and smectic C phases for short terminal chains ($m=1, 2$), a monotropic nematic phase for $m=4$, but then no mesophase formation until $m=9$ and 10, when a tilted ordered smectic G/J phase appears. This phase, for the odd parity spacer dimers, appears to have a modulated layer structure.

For the methylene-linked dimers with an even parity spacer ($n=6$), an enantiotropic nematic phase is formed for all lengths of terminal chains ($m=1–10$). For $m>4$, a tilted ordered smectic G/J phase appears below the nematic phase. This phase, for the even parity spacer dimers, appears to have a simple layer structure.

It thus appears that there is an odd–even effect in the structure of the ordered smectic G/J phases of the methylene-linked dimers, with a modulated layer structure being formed for the dimers with an odd

parity spacer ($n=5$), but a simple layer structure being formed for those with an even parity spacer ($n=6$). A somewhat similar odd–even effect was previously found in the *m*.O*n*O.*m* symmetric dimers (structure 3), where modulated hexatic phases were only observed for dimers with odd parity ($n=9$ or 11) spacers [30].

In order to clarify the detailed structures of the ordered smectic phases reported here for the ether-linked and methylene-linked dimers, it will be necessary to carry out XRD studies of macroscopically aligned samples. This should be achievable for the *m*O-6-O*m* dimers by magnetic alignment in the nematic phase, followed by careful cooling into the ordered smectic phase. This would allow us to discriminate between G and J phases, and directly measure the tilt angles. However, it may be more problematic to align the *m*O-5-O*m* dimers, partly because the ordered smectic phase forms directly from the isotropic phase, and partly because of the modulated layer structure we have inferred from the low angle powder diffraction data.

References

[1] C.T. Imrie, P.A. Henderson. *Curr. Opin. colloid inter. Sci.*, **7**, 298 (2002).
[2] C.T. Imrie. *Struct. Bond.*, **95**, 149 (1999).
[3] C.T. Imrie, G.R. Luckhurst. In *Handbook of Liquid Crystals*, vol. 2B, D. Demus, J.W. Goodby, G.W. Gray, H.W. Spiess, V. Vill (Eds), p. 801, Weinheim, Wiley-VCH (1998).
[4] C.V. Yelamaggad, M. Mathews, U.S. Hiremath, G.G. Nair, D.S. Shankar Rao, S.K. Prasad. *Liq. Cryst.*, **30**, 899 (2003).
[5] P.A. Henderson, A.G. Cook, C.T. Imrie. *Liq. Cryst.*, **31**, 1427 (2004).
[6] C.V. Yelamaggad, M. Mathews. *Liq. Cryst.*, **30**, 125 (2003).
[7] C.V. Yelamaggad, U.S. Hiremath, S.A. Nagamani, D.S. Shankar Rao, S.K. Prasad, N. Iyi, T. Fujita. *Liq. Cryst.*, **30**, 681 (2003).
[8] C.V. Yelamaggad, M. Mathews, T. Fujita, N. Iyi. *Liq. Cryst.*, **30**, 1079 (2003).
[9] J.-W. Lee, J.-I. Jin, M.F. Achard, F. Hardouin. *Liq. Cryst.*, **30**, 1193 (2003).
[10] A.T.M. Marcelis, A. Koudijs, Z. Karczmarzyk, E.J.R. Sudhölter. *Liq. Cryst.*, **30**, 1357 (2003).
[11] Y.S. Park, K.-H. Lee, J.-W. Lee, J.-I. Jin. *Liq. Cryst.*, **30**, 173 (2003).
[12] R. Achten, A. Koudijs, Z. Karczmarzyk, A.T.M. Marcelis, E.J.R. Sudhölter. *Liq. Cryst.*, **31**, 215 (2004).
[13] S. Diez, D.A. Dunmur, M.R. de la Fuente, P.K. Karahaliou, G. Mehl, T. Meyer, M.A.P. Jubindo, D.J. Photinos. *Liq. Cryst.*, **30**, 1021 (2003).

[14] N. Olsson, I. Dahl, B. Helgee, L. Komitov. *Liq. Cryst.*, **31**, 1555 (2004).

[15] A. del Campo, A. Meyer, E. Pérez, A. Bello. *Liq. Cryst.*, **31**, 109 (2004).

[16] S.-L. Wu, S. Senthil. *Liq. Cryst.*, **31**, 1573 (2004).

[17] I. Nishiyama, J. Yamamoto, J.W. Goodby, H. Yokoyama. *Liq. Cryst.*, **31**, 1495 (2004).

[18] A.P.J. Emerson, G.R. Luckhurst. *Liq. Cryst.*, **10**, 861 (1991).

[19] A. Ferrarini, G.R. Luckhurst, P.L. Nordio, S.J. Roskilly. *J. chem. Phys.*, **100**, 1460 (1994).

[20] G.R. Luckhurst. In *Recent Advances in Liquid Crystalline Polymers*, Chap. 7, L.L. Chapoy (Eds), Elsevier (1985).

[21] A. Ferrarini, G.R. Luckhurst, P.L. Nordio, S.J. Roskilly. *Chem. Phys. Lett.*, **214**, 409 (1993).

[22] A. Ferrarini, G.R. Luckhurst, P.L. Nordio, S.J. Roskilly. *Liq. Cryst.*, **21**, 373 (1996).

[23] P. Barnes, A.G. Douglass, S.K. Heeks, G.R. Luckhurst. *Liq. Cryst.*, **13**, 603 (1993).

[24] P.A. Henderson, O. Niemeyer, C.T. Imrie. *Liq. Cryst.*, **28**, 463 (2001).

[25] R.W. Date, C.T. Imrie, G.R. Luckhurst, J.M. Seddon. *Liq. Cryst.*, **12**, 203 (1992).

[26] P. Keller, L. Liebert. In *Solid State Physics*, Vol. 14, H. Ehrenreich, F. Seitz, D. Turnbull, L. Liebert (Eds), Chap. 2, Academic Press, New York (1978).

[27] H. Dietze. PhD thesis, University of Halle (1922).

[28] D. Vorländer. *Z. Phys. Chem.*, **126**, 449 (1927).

[29] A.E. Blatch, G.R. Luckhurst. *Liq. Cryst.*, **27**, 775 (2000).

[30] R.W. Date, G.R. Luckhurst, M. Shuman, J.M. Seddon. *J. Phys. II Fr.*, **5**, 587 (1995).